Carbon 260 (2026) 121977

Contents lists available at ScienceDirect

Carbon

journal homepage: www.elsevier.com/locate/carbon

One-step fabrication of diamond microtubes: A proof of concept

J. Millán-Barba [a,b,*], F. Lloret [a,b], P. Pobedinskas [c,d], K. Haenen [c,d], D. Araujo [b,e]

[a] Department of Applied Physics, University of Cadiz, Puerto Real, Spain
[b] IMEYMAT, Puerto Real, Spain
[c] IMOMEC, IMEC vzw, Diepenbeek, Belgium
[d] Institute for Materials Research (IMO), Hasselt University, Diepenbeek, Belgium
[e] Department of Materials Science, Metallurgical Eng. & Inorganic Chem., University of Cadiz, Puerto Real, Spain

ARTICLE INFO

Keywords:
Microtubes
Diamond
Polycrystalline
Fabrication

ABSTRACT

A one-step methodology for the synthesis of diamond microtubes is proposed. Starting from carbon fibre (CF) substrates, diamond microtube is grown by Microwave Plasma Enhanced Chemical Vapour Deposition (MW PE CVD). Thanks to the graphitic nature of the CF, the substrate decomposition process (etching) takes place at the same time as the diamond layer grows on the CF substrate surface. The balance between the diamond growth rate and the CF etching is the key to obtain self-supporting microtubes. In addition, the nanodiamond seeding pre-treatment prior to MW PE CVD growth has been shown to play a main role in the process, adjusting the relationship between diamond growth and carbon etching. This work is a proof of concept of the diamond microtube fabrication, in which the formation process and morphology of the diamond microtubes are structurally evidenced by Scanning Electron Microscopy, while Raman spectroscopy and High-Resolution Transmission Electron Microscopy allow to demonstrate the diamond nature of the microtubes.

1. Introduction

Microtubes are used in biomedical applications acting as components in diagnostics equipment, mono-dispenser drop [1], or electrodes [2–4]. Techniques such as Lab-on-a-Chip (LOC) [5] or micro Total Analysis Systems (μTAS) [6,7] require micro elements, like microtubes, for a precise control and manipulation of fluids and particles in a micro scale size. For this purpose, several methods have been reported for creating tubular capillary structures. For example, polycaprolactone microtubes (15 – 30 μm) are used to deliver effective drugs for most central neural system disorders [8]. Other authors use titania microtubes implanted in the brains of rodents to supply drugs, although integrity, acceptance of the implant and immunohistochemistry were only assessed during the six months of implantation [9]. Microtubes can even be integrated into biosensors carrying fluids to detect biological and chemical molecules with high sensitivity [10]. Nevertheless, most of the base materials of these microtubes, such as silver [11] or silicon [12], present significant disadvantages in terms of biocompatibility and long-term stability. Silver is susceptible to oxidation, which limits its use in biomedical applications, and silicon, which also oxidises, can be brittle and susceptible to degradation in certain environments.

In the field of biomedical applications, the biocompatibility of materials is crucial to prevent inflammatory responses or rejection by the organism. Diamond stands out as an exceptional candidate due to its excellent biocompatibility [4], hardness, thermal conductivity, low coefficient of thermal expansion, chemical inertness and wear resistance [13], overcoming limitations of conventional materials such as titanium or stainless steel [14,15]. Furthermore, when appropriately doped with boron, diamond can acquire conductive properties making it a versatile material for electronic applications and biosensors. Semiconducting properties or even metallic-like electrical conduction can be achieved in diamond [16,17], while maintaining its biocompatible properties [18]. This unique combination of biocompatibility and tuneable electrical conductivity makes diamond a promising material for brain-machine interfaces and implantable medical devices, offering solutions to challenges presented by other materials in terms of longevity and stability in biological environments [19–21]. For example, boron-doped diamond microtubes could be used for applications as drug delivery [9], neuronal stimulation [22], or biomolecule sensing [23].

Other useful functions that microtubes can perform include heat

* Corresponding author. University of Cádiz, Dpto. Applied Physics, CASEM, Office 23, Wing C, 1a Floor, Puerto Real, Cádiz, P.C.:11510, Spain.
E-mail address: Josue.millan@gm.uca.es (J. Millán-Barba).

https://doi.org/10.1016/j.carbon.2026.121977
Received 6 April 2026; Received in revised form 29 July 2026; Accepted 10 August 2026
Available online 11 August 2026
0008-6223/© 2026 The Authors. Published by Elsevier Ltd. This is an open access article under the CC BY-NC-ND license (http://creativecommons.org/licenses/by-nc-nd/4.0/).

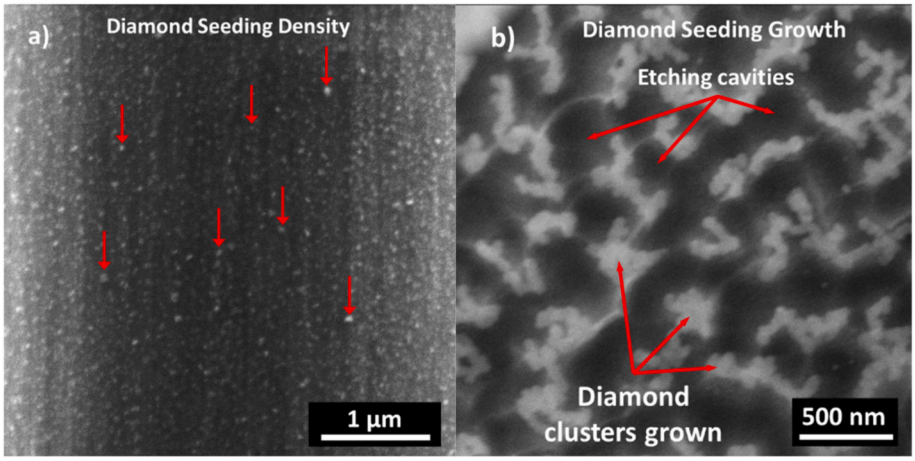


Fig. 1. SEM micrographs of a) diamond nanoparticles seeding density on CF surface (some diamond seed grains agglomerations are marked by red arrows), and b) diamond clusters grown on CF after 10 h growth by MW PE CVD. Etching craters on the CF surface (grey) between diamond clusters grown (white) are observed and marked with red arrows. (For interpretation of the references to colour in this figure legend, the reader is referred to the Web version of this article.)

transfer [24,25], waveguides [26] and needle fabrication [27,28]. Diamond offers a solution in areas such as microfluidics or microelectronics. For instance, the high surface-to-volume ratio of microtubes facilitates exceptional high heat transfer efficiency [29–31] that, combined with diamond's high thermal conductivity, can allow the development of compact heat exchangers for electronic devices. This feature is especially valuable for applications that require efficient thermal management in limited spaces. On the other hand, diamond microneedles can be used to produce free-standing diamond (100) crystal, as demonstrated by Koyama et al. [28]. Their method involves the continuous growth of a diamond layer on the top of a pattern of sufficiently close diamond microneedles, followed by a controlled cooling phase, which induces strain-induced breakage of the microneedles. This causes those microneedles to fracture creating free-standing diamond layer. Finally, electrically conductive boron-doped diamond microtubes have demonstrated significant potential in electrochemical sensing of drugs, organic compounds or heavy metals [32].

Nevertheless, diamond microtubes fabrication is still a challenge. Mainly, they have been reported to be fabricated in a two-steps process. This process uses a wolfram made microtube substrate upon which diamond is grown by chemical vapour deposition (CVD). Once the microtubes are covered by diamond, the substrate is removed by a chemical etching. This is a two-step process: 1. growth and 2. etching [33,34]. By this method, 30 mm long diamond microtubes are reached on a wolfram wire while hydrogen peroxide is used for the substrate etching [35–38]. Authors use microwave plasma enhanced (MWPE) CVD system for the diamond growth [33]. However, this process requires a significantly longer growth time (about 24 h) compared to the 7-16 h required for hot filament (HF) CVD system. To be followed by a further lengthy process (24 h) to remove the tungsten substrate, which increases the manufacturing costs. In addition, in terms of operational functionality, the internal roughness (Ra) of the resulting microtubes reduces the fluid flow. The manufacturing process of microtubes using a mould (fibres or wires) ensures that the inner wall of the microtube will replicate the roughness of the mould.

To reduce the required fabrication time, a one-step process has been developed using a copper-coated graphite wire as substrate and a HFCVD reactor to grow the diamond and etch the substrate at the same time [39]. Despite this innovative improvement, microtubes only reach lengths of tens of microns and may contain copper residues, which makes it non-biocompatible [40]. This makes this method unsuitable for biomedical applications.

To overcome the manufacturing and biocompatibility challenges associated with previous methods, this work uses carbon fibre (CF) as substrate on which boron-doped diamond (BDD) microtubes are fabricated in a one-step process. Here, the polycrystalline diamond microtubes are grown at the same time as the CF substrate is etched. The feasibility of BDD growth on CF by MW PE CVD has previously been described [41], where several observations arise from the growth conditions. At low temperature, the etching process is faster than diamond growth, while at high temperature it is opposite. Properly tuning those parameters one can reach CF etching at the same time allowing diamond growth. Then, the internal surface of the grown tube is as flat as that of the CF support. In addition, to promote the diamond growth, diamond seeding pre-treatment is used. Typically, diamond seeds are used for two objectives: (i) to promote the diamond growth and (ii) to act as protective layer against degradation of the substrate by hydrogen plasma. Therefore, the seeding density in the CF needs to be controlled to allow for degradation of the substrate while growing the diamond microtube.

This work is a proof of concept of a one-step diamond microtube fabrication process. The growth process and morphology of the diamond microtubes are revealed by Scanning Electron Microscopy (SEM) observations. The diamond nature of the polycrystalline microtubes was determined using High-Resolution Transmission Electron Microscopy (HR-TEM), and the diamond phase purity (sp^3/sp^2 carbon ratio) and boron doping incorporation has been evidenced by Raman spectroscopy.

2. Methodology

Commercial polyacrylonitrile (PAN) CFs ''HexTow AS7'' (from Hexcel corporation) were used as a substrate for the diamond microtube formation. The AS7 CFs were in tow format, which is a narrow tape of 12,000 CFs filaments arranged in the same direction with ~5 cm length, where each CF has a diameter of 6.9 µm. The tow substrate was diamond seeded by the immersion of the tow in a solution of diamond nanoparticles in DI water [42,43]. Diamond growth was performed over one tow using MW PE CVD in a clamshell ASTeX 6500 series system [44]. A gas mixture of methane, hydrogen and trimethylboron (TMB, diluted in H_2 at 1000 ppm) was used in a proportion of 5 sccm, 455 sccm and 40 sccm, respectively. The B/C ratio was 8000 ppm. The working pressure and MW power were set at 35 Torr and 3.5 kW, and the growth time was 10 h. The tow was held in the reactor chamber with a homemade Mo holder. The temperature was estimated in a range between 650 and 1200°C along the CF tow, measured by a single-color optical pyrometer with the emissivity set to 0.6. The broad temperature range is attributable to the fact that the 12,000 tow fibres, with a length of 5 cm, are subjected to varying temperatures in accordance with their respective positions relative to the plasma zone. Consequently, CFs closer to the



Fig. 2. CF tow inside a MW PE CVD chamber during a diamond growth process. The different colours of the CFs that compounds the tow evidence the wide range of temperature of the CFs substrates. (For interpretation of the references to colour in this figure legend, the reader is referred to the Web version of this article.)

interior of the plasma with higher energy density experience more heating than CFs inside the tow.

The seeding pre-treatment and the resulting sample from the diamond growth were observed by scanning electron microscopy (SEM) using a Solaris Tescan UHR FESEM FIB microscope to analyse its morphology. For the compositional study of the microtube, MicroRaman spectrometry was performed using LabrRAM HR spectrometer from Horiba Jobin-Yvon interfaced to an Olympus microscope. The excitation wavelength was 488 nm. The spectrometer was calibrated using the silicon F1g peak at 520.2 cm^{-1}. The raw Raman spectra were corrected for instrumental response, the temperature effect, and the frequency factor as described in Ref. [45]. The sp^3/sp^2 carbon bond ratio content was estimated from Raman spectra using the method described by Fortunato et al. [46]. The area intensities of the peaks and bands were obtained from a Raman spectrum multipeak deconvolution using the Lorentzian function by Origin© 2018 software.

In addition, HR-TEM study of the microtube composition was carried out by a TEM lamella of the polycrystalline microtube, which was prepared using an FEI Scios 2 DualBeam focused ion beam/scanning electron microscope (FIB/SEM) equipment. Subsequent high-resolution transmission electron microscopy (HR-TEM) characterization was performed using an FEI Talos F200X microscope.

3. Results and discussion

Diamond nanoparticles seeding has been used as pre-treatment on the CF surface prior to diamond growth. After the nanodiamond seeding pre-treatment, a homogenous distribution of the diamond nanoparticle agglomerations can be observed in Fig. 1(a) by SEM. Together the seeding nanoparticle agglomerations, in the raw CF surface is observed longitudinal grooves characteristics of the manufacturing process [47]. The diamond seeding agglomerations, seen as small white dots on the surface and marked by red arrows, are covering between 28% and 40% of the total CF surface ($12.9 \cdot 10^3 \pm 0{,}3$ agglomerated seed particles/cm^2). Take into account, that in addition to the observed seeding particle agglomerations covering the CF, individual nanoparticles below the SEM resolution are also deposited. The diamond seeding density affects the CF etching process acting as a barrier for the plasma to reach the CF surface and eliminate the substrate. This range of seeding density was optimised to achieve a balance between diamond growth and CF etching to obtain the microtubes.

The seeded CF tow was introduced into the MW PE CVD system for the diamond growth where the diamond nanoparticles begin to grow while the hydrogen species of the plasma etch the CF. The etching process starts on the non-covered areas of the CFs surface, generating cavities around the diamond grains. It is known that diamond seeds nanoparticles are subject to etching in the early stages of growth, reducing the coating density on the surface of the CF [48]. The surviving nanoparticles and their agglomerates, together with the carbon nanowall formations generated during the diamond growth process on CF described in previous work [49], serve as the nucleation sites for the polycrystalline microtube. Fig. 1(b) shows a SEM micrograph of a CF where the growth conditions were not sufficient to achieve a high growth and etching rates to produce a microtube after 10 h. Etching craters and diamond clusters grown are visible by the white-black contrast and they are marked on the figure. This image is correlated with the initial state of microtube formation.

Making an interjection about the description of the microtube formation process, a question arises as to why CFs as illustrated in Fig. 1 (b) and microtubes (covered subsequently in the manuscript) are obtained in a single process after 10 h? In response, Fig. 2 shows the different temperatures that reach the CFs of the tow during a diamond grow process in the MW PE CVD system. This temperature difference can be attributed to two primary reasons: (i) The CFs, constituting a discontinuous set of 12,000 units (a tow), exhibit non-uniform dispersion. This is due to the fact that, during the manipulation and seeding process, the filaments extend beyond the confines of the tow surface. The substrate temperature undergoes variation from the top CFs, which have higher temperature due to its proximity to the zone with the highest energetic density of the plasma, to the inner CFs of the tow. This variation gives rise to changes in the diamond growth and CF etch rates, thus enabling the observation of different growth results in a single attempt. This is caused by the uneven temperature (650 – 1200°C) of the CF filaments across the tow. Consequently, the filaments that protrude attain a higher temperature of 1200°C, while the filaments further away from the plasma reach a lower temperature of up to 650°C. (ii) In addition, the

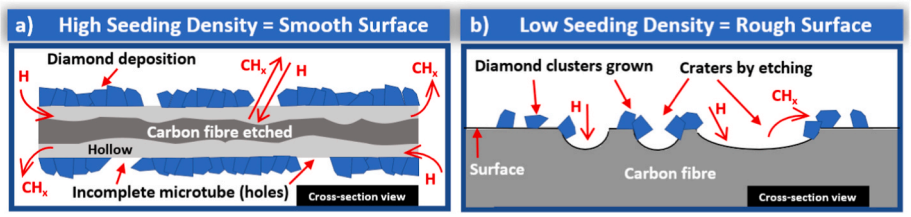


Fig. 3. a) Diagram of the MWPECVD polycrystalline diamond microtube formation process on a CF with a high diamond seeding density (28%-40% of the surface). The bare CF is shown in light grey, and the CF etched in dark grey. b) Diagram showing diamond growth on a CF and the CF etching process on a low diamond seeding density CF.

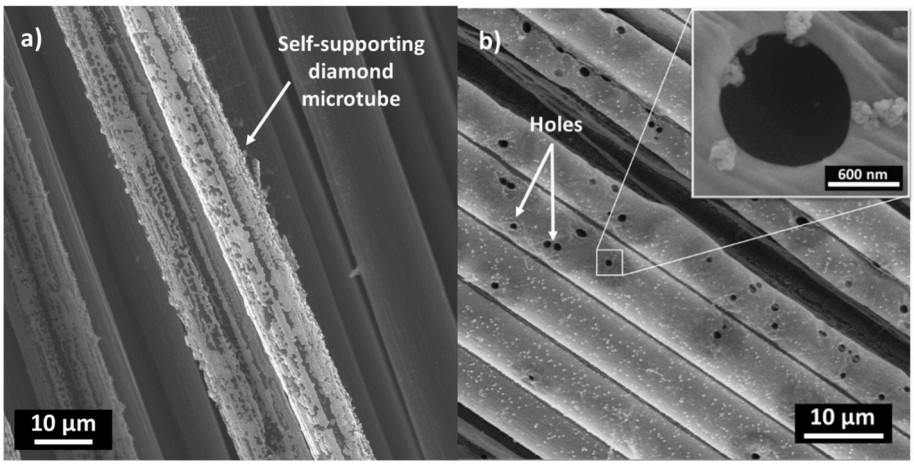


Fig. 4. Micrographs of cylindrical incomplete self-supporting polycrystalline diamond microtube at a) with an advanced stage of diamond microtube formation where the deteriorated substrate continues to remain in the interior, and b) almost fully formed microtubes with some holes in the surface. The inset in b) shows an individual hole in the polycrystalline diamond layer.

plasma shadow effect caused by the tow CFs among them. By this effect the CFs above and closer to the high-energy density zone of the plasma act as a barrier, reducing the energy density of the plasma that reach the CFs inside the tow, thereby reducing its temperature. However, not only changes the CF's temperature, but it also results in a decrease in plasma species density as it penetrates the tow, affecting the growth and etch rates. CFs placed in the outer zone of the tow receive higher number of species from the plasma, while the inner CFs of the tow are hidden by external CFs. CF filaments closer to the plasma create different growth and CF etch rates in the subsequent CFs without direct contact with the plasma.

The microtube formation from the CFs is a process affected by the diamond growth and CF etch rates. Depending on these rates the microtube formation reaches its complete form. In turn, these rates depend mostly on the substrate temperature as shown in Figs. 1 and 2, and thus in the proximity of the CFs to the plasma and the shading effect of the CFs. As both rates are proportional mostly to the temperature, influenced by the position of the CF relative to the plasma and other CFs under identical growth conditions (MW power, pressure, gas mixture, etc.), it can be observed that at low growth and etch rates obtained in the CFs at the lowest temperatures (∽650°C), it can be observed the initial stage of the diamond formation in Fig. 1(b).

Continuing with the analysis of microtube formation, Fig. 3(a) shows a diagram of the diamond microtube formation process where a high diamond density is used, and the diamond growth is fast enough to form a self-supporting tube before the CF disappears. As a result, the internal roughness of the microtube is the same as the CF surface. However, when a low seeding density is used (Fig. 3(b)), the diamond growth rate is not sufficient to completely cover the CF, but the CF etching occurs, resulting in a non-flat grown layer or a non-self-supporting microtube. Finishing in higher roughness on the inner surface of the microtube.

By focusing on zones of the tow with CFs at an intermediate temperature during the growth process (higher than in the CF of Fig. 1(b)), the diamond growth and CF etching rates increase. The clusters of diamond grains become larger and begin to bond together, forming an irregular diamond layer with void areas or holes. At this point, the polycrystalline diamond layer begins to be self-supporting, but it is not completely closed so the remaining graphite of the CF can still be etched by its exposure to the plasma (Fig. 4(a)). Once the diamond nanotube is almost closed, the few gaps left allow us to verify that the tube is empty (Fig. 4(b)). The inside of the tube is emptied thanks to the hydrogen that enters through the micro holes and through the tube inlets, forming volatile CH_x. The micro holes observed in the inset of Fig. 4(b) are then filled out as the diamond growth rate increases.

Finally, analysing one of the resulted formations located with the highest temperature zones during the process (900 – 1200°C), a microtube is obtained. For higher diamond growth and etching rates, the process produces a tubular structure in which the CF substrate has been completely eliminated. With the tube completely closed, its interior remains isolated from the plasma and, therefore, the diamond cannot

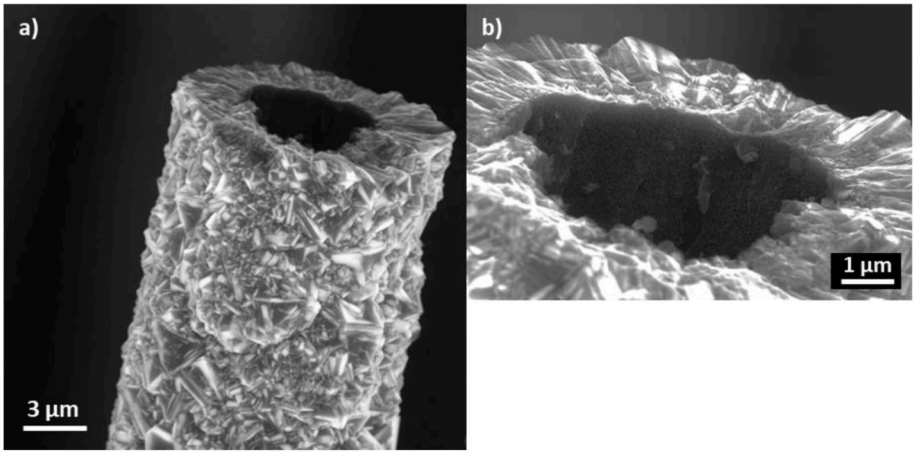


Fig. 5. Micrographs of a) polycrystalline boron-doped diamond microtube with micro grain size, and b) an enlargement from the microtube end.

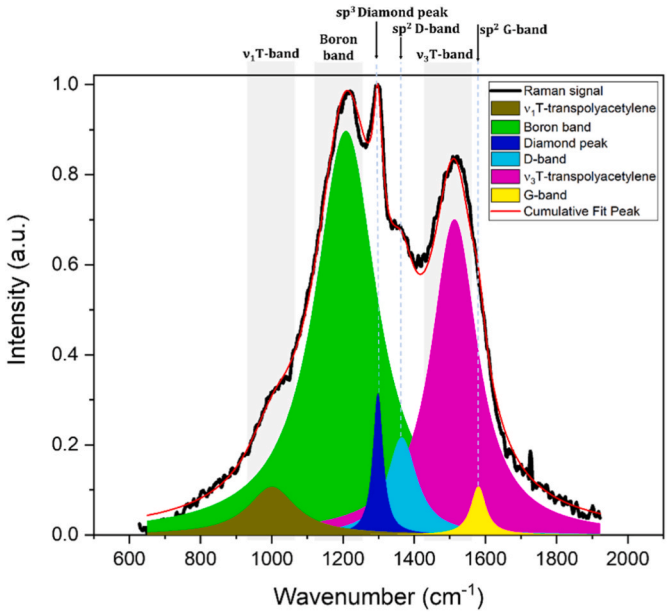


Fig. 6. Raman spectrum signal (black line) obtained on a BDD microtube. Peaks and bands (coloured deconvolution) were deconvoluted using the Lorentzian function to generate the cumulative fitting curve (red line). (For interpretation of the references to colour in this figure legend, the reader is referred to the Web version of this article.)

grow on that side. This process results in a hollow diamond tube, shown in Fig. 5(a). Evidence confirming the hollow nature of the microtubes is provided in Fig. S1 of the Supplementary Information. The growth conditions used here and the CF temperature after 10 h allows the balance between the diamond growth and the CF etching rates, reaching a microcrystalline size of diamond grains. The resulted microcrystalline diamond tube has an outer diameter of 13.0 ± 0.1 μm, and an inner diameter of ∽6.9 μm. The inner diameter matches the nominal diameter of the CF, suggesting that it has been fully etched. A magnification of the end of the microtube in Fig. 5(b) shows the inner face of the tube.

As a result of a balance between the diamond growth and the etching rates, diamond microtubes from CF substrates are formed. In this way, the diamond growth rate is fast enough in relation to the CF etching that it allows to form a polycrystalline cylindrical diamond layer self-supporting before the CF collapses and loses its shape. The estimated diamond growth rate was ∽650 nm/h, as determined by the SEM measurement of the wall thickness of the diamond microtube and dividing it by the total growth time. The obtained growth rate is framed within the growth rate range of the references cited here, which is 250 – 7800 nm/h [33–39]. Regarding the CF etching rate, it has been demonstrated that is also affected by the substrate temperature [50,51]. Otherwise, the complete CF etching prevented a more accurate determination of the actual etching rate for the diamond microtube formation. Nonetheless, the minimum rate was estimated by dividing the CF radius (3.45 μm) by the total growth time (10 h), giving a value of at least 350 nm/h. This etching rate in graphite have been reported at temperatures of around 450°C in a hydrogen plasma [50,52,53]. Additionally, graphite etching rate of over 100 μm/h have been reported in hydrogen plasma with a substrate temperature of 900°C and a pressure of 155 mbar [51]. The successful fabrication of diamond microtubes depends on the critical balance between diamond growth and CF etching rates. This ratio was estimated as 1.9, diamond deposition exceeding CF etching, enabling the formation of uniform tubular structures. A lower ratio, where the CF etching rate approaches or exceeds the growth rate, would lead to premature CF shape loss before diamond grains could form a self-supporting structure. Such an imbalance would result in non-uniform diamond structures, compromising the integrity and desired tubular morphology of the final microtube.

The advantage of producing diamond microtubes in one-step process is due to the composition of the CFs. These are composed of two-dimensional graphitic (sp^2-carbon bonds) turbostratic carbon sheets, with crystalline and amorphous carbon phases. The packaging of the graphitic sheets promotes the formation of ribbons following the fibre axis direction [54]. When CFs are immersed in a harsh environment, such as hydrogen plasma during the MWPECVD diamond growth process, they decompose. Hydrogen plasma produces hydrogen species that interact with the carbon atoms of the CF surface, resulting in etching of the material. This is because hydrogen species have a preference for eliminating the sp^2 carbon bond, which favours the formation of the sp^3 carbon bond formation (diamond). The graphite decomposition process takes place at the same time as the diamond layer is formed on the CF surface. Therefore, it is possible to end up with a diamond microtube in a one-step process. As a consequence of the ratio between diamond growth rate and CF substrate etching, the microtube is formed.

To determine the quality of the diamond, an analysis of the composition of the microtube was carried out by Raman spectroscopy. Fig. 6 shows the Raman spectrum obtained on the microtube (black curve). Lorentzian deconvolution of the signal is used to calculate the area and position of the peaks and bands. The sp^3 carbon bond peak corresponding to diamond is identified at 1300 cm^{-1} (dark blue in the deconvolution). The standard position for the diamond peak is 1332 cm^{-1}. This displacement to lower energies observed is attributed to boron inclusion in the diamond lattice, the phonon confinement, the electronic Raman interaction and the grain size [55,56]. The Raman results confirm the diamond composition of the microtube as well as the heavily boron incorporation to its lattice network. The presence of boron atoms has been shown to induce a Fano effect, whereby interference is produced between the diamond peak and the continuum of electronic excitations [55,57,58]. Raman spectrum (Fig. 6) shows broad band located at 1208 cm^{-1} (green in the deconvolution) attributed to the boron contribution. Boron, in substitutional position within the diamond lattice [57,59], has been shown to produce a broad band with a maximum value around the 1200 cm^{-1} position [56,60,61].

The characteristic peaks of disordered carbon sp^2-bonds (amorphous carbon) appear as a small shoulder to the right of the diamond peak (1365 cm^{-1}, as light blue in the deconvolution), in the case of the D-band, and at 1580 cm^{-1} for the G-band (yellow in the deconvolution). Peak ν_1 at 1000 cm^{-1} (gold in the deconvolution) is attributed to the C-H in plane bending, and ν_3 at 1510 cm^{-1} (pink in the deconvolution) to C═C stretch, indicating transpolyacetylene segments present at the surface and the grain boundaries of the diamond layer [62].

The boron concentration in diamond can be estimated using the method of the double Fano effect proposed by Mortet et al. [55,56,59,63] on the Raman spectrum. This method is based on a combination of electronic Raman scattering modelling and multiple Fano-functions. The position and width of the boron band and diamond peak attributed respectively to the Fano-shaped maximum of phonon density of states and zone-centre phonon line of heavily boron-doped diamond, can be used to determine the atomic boron concentration. The method fits the boron-doped diamond Raman spectrum to obtain the width of the diamond peak the fitting function reported in Ref. [55]. Subsequently the diamond peak width is correlated to the boron concentration by a linear function obtained by comparing the width of the diamond peak with its boron concentration, as determined by secondary ion mass spectrometry [63]. Accordingly, the boron concentration is estimated to be in the range of $10^{21} cm^{-3}$.

To determine the diamond quality, a factor f_q was calculated to indicate the sp^3/sp^2 carbon ratio [64]. The intensities areas of diamond peak, G-band, and D-band from Raman spectrum result have been used (Fig. 6). They are 15 ± 1, 8 ± 2 and 34 ± 3, respectively, and the factor f_q is calculated by next equation (1):

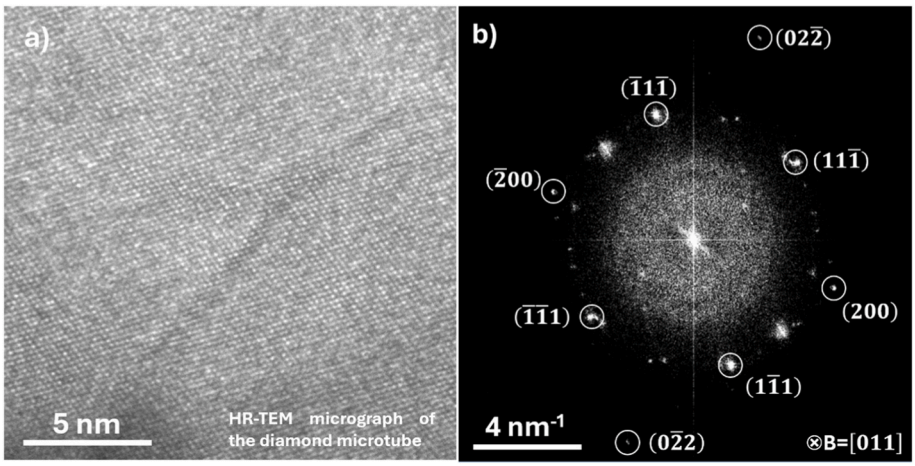


Fig. 7. TEM micrograph of a polycrystalline diamond microtube. (a) HR-TEM micrograph shows the crystalline nature of the microtube, and (b) FFT pattern of (a) micrograph showing the dominant crystallographic orientations corresponding to [011] zone axis for the fcc diamond crystal (spots indexed and marked by white circumferences).

$$f_q = \frac{75 \times I_d}{(75 \times I_d) + \left(\sum_{nd} I_{nd}\right)} \times 100 \quad (1)$$

where $\sum_{nd} I_{nd}$ is the sum of Raman sp^2 phase peak areas (G- and D-bands), and I_d is the Raman diamond peak area (sp^3-bond peak). The 75 factor considers the more effective Raman scattering of the sp^2 structures [46]. Using this equation, the f_q factor obtained is ~96%. Which is equivalent to 96% of sp^3 carbon bonds attributed to diamond and confirming the high diamond quality. Although no absolute indication of purity is achieved, the f_q factor makes it possible to classify films according to their quality.

To clarify the diamond nature of the polycrystalline microtube and verify the Raman spectrum result, a High-Resolution Transmission Electron Microscopy (HR-TEM) study was carried out. Fig. 7 shows some HR-TEM results: a micrograph at high magnification (Fig. 7(a)) of a TEM lamella obtained from a polycrystalline microtube, and the Fast Fourier Transform (FFT) from the mentioned micrograph (Fig. 7(b)). In Fig. 7 (a), well-defined lattice fringes confirm the crystallinity. In the FFT pattern (Fig. 7(b)), the presence of various discrete spots resulting from different crystallographic reflections can be observed, which were indexed along the fcc crystal in the [011] zone axis [65]. The d-spacing of the main marked spots from the polycrystalline diamond was measured, confirming the family planes {111} [66]. Therefore, comparing the theoretical and experimental d-spacing, the polycrystalline microtubes are unequivocally attributed to diamond (Further information can be found in Supplementary Information, which presents a more detailed HR-TEM compositional analysis of a section extracted from a microtube, as shown in Fig. S2).

To determine the efficiency of the process, a representative area of the sample was examined. Five microtubes were found in these regions, verified one by one by FIB/SEM equipment, out of 1442 fibres, which gives a formation efficiency of 0.35%. The origin of such low efficiency of microtube formation is the non-homogeneous conditions during the CVD process, where the temperature fibre dispersion was estimated from 650°C to 1200°C.

4. Conclusion

By combining the susceptibility of the CF to the diamond CVD plasma (or phenomena of etching by CVD hydrogen plasma) and adjusting the growth rate of diamond we have achieved a heavily boron-doped polycrystalline diamond (BDD) microtubes with diameters of approximately 13 μm and lengths of tens of microns. This one-step CVD process on a CF substrate has several advantages over the traditional two-step and one-step with copper methods. Not only is it less time consuming, it eliminates the need to remove the cylindrical substrate by chemical etching after the diamond growth, while also reducing contamination in the diamond tubes.

The CF substrate temperature during the diamond growth plays a major role. Since only in the zones where the CFs were at a higher temperature, polycrystalline diamond microtubes have been generated. This reduces the efficiency in the microtube formation, where only the top CFs with higher temperature allow the balance between the diamond growth and CF etching rates to produce a diamond microtube. The rest of the CFs did not have enough growth and etching rates to achieve microtube formation. Although the process efficiency is low, 0.35%, this limitation can be addressed by implementing positioning strategies of the CF substrate through specific holder designs and optimizing growth conditions to achieve homogeneous conditions across the entire substrate. Furthermore, the spacing between individual CFs must be sufficient to prevent plasma shadowing effects, thereby ensuring homogeneous etching and growth conditions throughout the entire tow.

Consequently, the one-step diamond microtube fabrication method presented here has been demonstrated using CF as substrate and a MW PE CVD system, validating the proof of concept. The versatility of BDD microtubes should be highlighted, as their electrical and thermal conductivities, hardness and structure offer promising potential for a wide range of microfluidic and electrode applications. This opens up new opportunities for future research and applications.

CRediT authorship contribution statement

J. Millán-Barba: Conceptualization, Data curation, Formal analysis, Investigation, Methodology, Validation, Writing – original draft. **F. Lloret:** Conceptualization, Data curation, Formal analysis, Funding acquisition, Investigation, Methodology, Project administration, Resources, Supervision, Validation, Writing – review & editing. **P. Pobedinskas:** Data curation, Formal analysis, Funding acquisition, Methodology, Resources, Supervision, Writing – review & editing. **K. Haenen:** Funding acquisition, Resources, Writing – review & editing. **D. Araujo:** Conceptualization, Formal analysis, Funding acquisition, Investigation, Project administration, Resources, Supervision, Writing – review & editing.

Declaration of competing interests

The authors declare that they have no known competing financial

interests or personal relationships that could have appeared to influence the work reported in this paper.

Acknowledgements

This work was funded through grants from the Spanish Ministry of Science, Innovation and Universities (PID2023-150076OB-I00, Green-JFET project, PDC2023-145907-I00, DiamChip project, and PID2020-117201RB-C21, OptoFET project). P. Pobedinskas and K. Haenen acknowledge the funding from the UHasselt Special Research Fund (BOF) via the Methusalem NANO network.

Appendix A. Supplementary data

Supplementary data to this article can be found online at https://doi.org/10.1016/j.carbon.2026.121977.

References

[1] E.K. Sackmann, A.L. Fulton, D.J. Beebe, The present and future role of microfluidics in biomedical research, Nature 507 (2014) 181–189, https://doi.org/10.1038/nature13118.
[2] A. Rifai, E. Pirogova, K. Fox, Diamond, carbon nanotubes and graphene for biomedical applications, in: Encyclopedia of Biomedical Engineering, Elsevier, 2019, pp. 97–107, https://doi.org/10.1016/B978-0-12-801238-3.99874-X.
[3] W.C. Poh, K.P. Loh, W. De Zhang, S. Triparthy, J.-S. Ye, F.-S. Sheu, Biosensing properties of diamond and carbon nanotubes, Langmuir 20 (2004) 5484–5492, https://doi.org/10.1021/la0490947.
[4] K. Yang, R.J. Narayan, Biocompatibility and functionalization of diamond for neural applications, Curr. Opin. Biomed. Eng. 10 (2019) 60–68, https://doi.org/10.1016/j.cobme.2019.03.002.
[5] J. Zhang, S. Yan, D. Yuan, G. Alici, N.-T. Nguyen, M. Ebrahimi Warkiani, et al., Fundamentals and applications of inertial microfluidics: a review, Lab Chip 16 (2016) 10–34, https://doi.org/10.1039/c5lc01159k.
[6] R. Keçili, S. Büyüktiryaki, C. Mustansar Hussain, Micro total analysis systems with nanomaterials, in: Handbook of Nanomaterials in Analytical Chemistry, 2020, pp. 185–198, https://doi.org/10.1016/B978-0-12-816699-4.00008-6.
[7] D.R. Reyes, D. Iossifidis, P.-A. Auroux, A. Manz, Micro total analysis systems. 1 . Introduction, theory, and technology, Anal. Chem. 74 (2002) 2623–2636, https://doi.org/10.1021/ac0202435.
[8] D. Sooriyaarachchi, Y. Zhou, S. Maharubin, G.Z. Tan, Microtube-embedded microfluidic devices for potential applications in blood brain barrier research, Procedia Manuf. 48 (2020) 294–301, https://doi.org/10.1016/j.promfg.2020.05.050.
[9] T. Lopez, E. Ortiz-Islas, J. Manjarrez, F. Rodriguez Reinoso, A. Sepulveda, R. D. Gonzalez, Biocompatible titania microtubes formed by nanoparticles and its application in the drug delivery of valproic acid, Opt. Mater. 29 (2006) 70–74, https://doi.org/10.1016/j.optmat.2006.03.016.
[10] S. Sánchez, Lab-in-a-tube systems as ultra-compact devices, Lab Chip 15 (2015) 610–613, https://doi.org/10.1039/c4lc90121e.
[11] X. Yang, L. Wang, S. Yang, Facile route to fabricate large-scale silver microtubes, Mater. Lett. 61 (2007) 2904–2907, https://doi.org/10.1016/j.matlet.2007.01.006.
[12] D. Roque Huanca, H.Y. Kim, W.J. Salcedo, Silicon microtubes made by immersing macroporous silicon into ammonium fluoride solution, Mater. Chem. Phys. 160 (2015) 12–19, https://doi.org/10.1016/j.matchemphys.2015.03.032.
[13] J.H.T. Luong, K.B. Male, J.D. Glennon, Boron-doped diamond electrode: synthesis, characterization, functionalization and analytical applications, Analyst 134 (2009) 1965–1979, https://doi.org/10.1039/b910206j.
[14] L. Tang, C. Tsai, W.W. Gerbarich, L. Kruckeberg, D.R. Kania, Biocompatibility of chemical-vapour- deposited diamond, Biomaterials 16 (1995) 483–488.
[15] D.F. Williams, On the mechanisms of biocompatibility, Biomaterials 29 (2008) 2941–2953, https://doi.org/10.1016/j.biomaterials.2008.04.023.
[16] S. Koizumi, C. Nebel, M. Nesladek (Eds.), Physics and Applications of CVD Diamond, WILEY-VCH, Weinheim, 2008, https://doi.org/10.1002/9783527623174.
[17] J. Barjon, N. Habka, C. Mer, F. Jomard, J. Chevallier, P. Bergonzo, Resistivity of boron doped diamond, Phys. Status Solidi Rapid Res. Lett. 3 (2009) 202–204, https://doi.org/10.1002/pssr.200903097.
[18] M. Alcaide, A. Taylor, M. Fjorback, V. Zachar, C.P. Pennisi, Boron-doped nanocrystalline diamond electrodes for neural interfaces: in vivo biocompatibility evaluation, Front. Neurosci. 10 (2016), https://doi.org/10.3389/fnins.2016.00087.
[19] D.J. Garrett, K. Ganesan, A. Stacey, K. Fox, H. Meffin, S. Prawer, Ultra-nanocrystalline diamond electrodes: optimization towards neural stimulation applications, J. Neural. Eng. 9 (2012), https://doi.org/10.1088/1741-2560/9/1/016002.
[20] C.E. Nebel, B. Rezek, D. Shin, H. Uetsuke, N. Yang, Diamond for bio-sensor applications, J. Phys. D Appl. Phys. 40 (2007) 6443–6466, https://doi.org/10.1088/0022-3727/40/20/S21.
[21] P. Bergonzo, A. Bongrain, E. Scorsone, A. Bendali, L. Rousseau, G. Lissorgues, et al., 3D shaped mechanically flexible diamond microelectrode arrays for eye implant applications: the MEDINAS project, IRBM 32 (2011) 91–94, https://doi.org/10.1016/j.irbm.2011.01.032.
[22] B. Fan, C.A. Rusinek, C.H. Thompson, M. Setien, Y. Guo, R. Rechenberg, et al., Flexible, diamond-based microelectrodes fabricated using the diamond growth side for neural sensing, Microsyst. Nanoeng. 6 (2020), https://doi.org/10.1038/s41378-020-0155-1.
[23] P. Song, H. Fu, Y. Wang, C. Chen, P. Ou, R.T. Rashid, et al., A microfluidic field-effect transistor biosensor with rolled-up indium nitride microtubes, Biosens. Bioelectron. 190 (2021) 113264, https://doi.org/10.1016/j.bios.2021.113264.
[24] B.H. Salman, H.A. Mohammed, K.M. Munisamy, A.S. Kherbeet, Characteristics of heat transfer and fluid flow in microtube and microchannel using conventional fluids and nanofluids: a review, Renew. Sustain. Energy Rev. 28 (2013) 848–880, https://doi.org/10.1016/j.rser.2013.08.012.
[25] J. Cui, H. Kang, J. Dou, X. Dong, Z. Wang, Z. Fan, et al., High-quality fabrication of diamond straight microchannels heat sink with large aspect ratio microchannels using UV nanosecond laser based on multi-feed method, Opt Laser. Technol. 171 (2024) 110429, https://doi.org/10.1016/j.optlastec.2023.110429.
[26] P. Schoessow, A. Kanareykin, R. Gat, CVD diamond dielectric accelerating structures, AIP Conf. Proc. 1086 (2009), https://doi.org/10.1063/1.3080939.
[27] S.S. Mammana, M.C. Salvadori, K. Kawakita, M.T. Pereira, M. Cattani, Characterization of diamond sonic micronozzles and microtube, J. Vac. Sci. Technol. B: Microelectronics and Nanometer Structures 21 (2003) 2034, https://doi.org/10.1116/1.1603287.
[28] K. Koyama, S.-W. Kim, M. Yoshimoto, Influence of diamond-etching conditions on the fabrication of diamond microneedles by a thermochemical reaction of Ni in an $H_{2/s}$ atmosphere, J. Ceram. Soc. Jpn. 129 (2021) 481–484, https://doi.org/10.2109/jcersj2.21025.
[29] Z. Li, D.-X. Du, Z.-Y. Guo, Experimental study on flow characteristics of liquid in circular microtubes, Microscale Thermophys. Eng. 7 (2003) 253–265, https://doi.org/10.1080/10893950390219083.
[30] B. Meng, M. Wan, R. Zhao, Z. Zou, H. Liu, Micromanufacturing technologies of compact heat exchangers for hypersonic precooled airbreathing propulsion: a review, Chin. J. Aeronaut. 34 (2021) 79–103, https://doi.org/10.1016/j.cja.2020.03.028.
[31] K.D. Cole, B. Çetin, The effect of axial conduction on heat transfer in a liquid microchannel flow, Int. J. Heat Mass Tran. 54 (2011) 2542–2549, https://doi.org/10.1016/j.ijheatmasstransfer.2011.02.007.
[32] T. Kondo, Recent electroanalytical applications of boron-doped diamond electrodes, Curr. Opin. Electrochem. 32 (2022) 100891, https://doi.org/10.1016/j.coelec.2021.100891.
[33] S. Silva, M.C. Salvadori, K. Kawakita, M.T. Pereira, R.M. Galvão, M. Cattani, Diamond flow controller microtubes, J. Micromech. Microeng. 12 (2002) 108–110, https://doi.org/10.1088/0960-1317/12/2/302.
[34] A.K. Dua, D.D. Pruthi, V.C. George, P. Raj, Formation of self-supporting hollow diamond helix and diamond sieve using "jet-flow" HFCVD, Solid State Commun. 93 (1995) 759–762.
[35] P.W. May, C.A. Rego, R.M. Thomas, M.N.R. Ashfold, K.N. Rosser, N.M. Everitt, CVD diamond wires and tubes, Diam. Relat. Mater. 3 (1994) 810–813, https://doi.org/10.1016/0925-9635(94)90274-7.
[36] V. Baranauskas, H.J. Ceragioli, A.C. Peterlevitz, S.F. Durrant, Development of tubes of micro-crystalline diamond and diamond-like carbon, Thin Solid Films 398–399 (2001) 250–254, https://doi.org/10.1016/S0040-6090(01)01441-9.
[37] V. Baranauskas, H.J. Ceragioli, A.C. Peterlevitz, Fabrication of tubes of diamond with micrometric diameters and their characterization, Thin Solid Films 420–421 (2002) 151–154, https://doi.org/10.1016/S0040-6090(02)00790-3.
[38] V. Baranauskas, H.J. Ceragioli, A.C. Peterlevitz, Growth of self-supported diamond tubes in the hot-filament chemical vapor deposition system, Diam. Relat. Mater. 12 (2003) 346–349, https://doi.org/10.1016/S0925-9635(02)00284-4.
[39] A.A. Morrish, J.W. Glesener, M. Fehrenbacher, P.E. Pehrsson, B. Maruyama, P. M. Natishan, Diamond tubes and fibers, Diam. Relat. Mater. 3 (1993) 173–176, https://doi.org/10.1016/0925-9635(94)90053-1.
[40] L.M. Gaetke, H.S. Chow-Johnson, C.K. Chow, Copper : toxicological relevance and mechanisms, Arch. Toxicol. 88 (2014) 1929–1938, https://doi.org/10.1007/s00204-014-1355-y.
[41] J. Millán-Barba, M. Gutiérrez, F. Lloret, R. Guzmán de Villoria, R. Alcántara, K. Haenen, et al., Study of early stages in the growth of boron-doped diamond on carbon fibers, Physica Status Solidi (a) Applications and Materials Science 218 (2020), https://doi.org/10.1002/pssa.202000284.
[42] S.I. Shah, M.M. Waite, Diamond deposition on carbon fibers, J. Vac. Sci. Technol. A: Vacuum, Surfaces, and Films 13 (1995) 1624–1627, https://doi.org/10.1116/1.579741.
[43] M. Marton, M. Vojs, M. Kotlár, P. Michniak, Ľ. Vančo, M. Veselý, et al., Deposition of boron doped diamond and carbon nanomaterials on graphite foam electrodes, Appl. Surf. Sci. 312 (2014) 139–144, https://doi.org/10.1016/j.apsusc.2014.05.199.
[44] S.S. Nicley, S. Drijkoningen, P. Pobedinskas, J. Raymakers, W. Maes, K. Haenen, Growth of boron-doped diamond films on gold-coated substrates with and without gold nanoparticle formation, Cryst. Growth Des. 19 (2019) 3567–3575, https://doi.org/10.1021/acs.cgd.9b00488.
[45] V. Mortet, L. Kavan, A. Taylor, Z. Vl, D. Machon, O. Frank, et al., Analysis of heavily boron-doped diamond Raman spectrum, Diam. Relat. Mater. 88 (2018) 163–166, https://doi.org/10.1016/j.diamond.2018.07.013.

[46] W. Fortunato, A.J. Chiquito, J.C. Galzerani, J.R. Moro, Crystalline quality and phase purity of CVD diamond films studied by Raman spectroscopy, J. Mater. Sci. 42 (2007) 7331–7336, https://doi.org/10.1007/s10853-007-1575-0.
[47] R. Ruan, W. Cao, L. Xu, Quantitative characterization of physical structure on carbon fiber surface based on image technique, Mater. Des. 185 (2020) 108225, https://doi.org/10.1016/j.matdes.2019.108225.
[48] R. Salerno, B. Pede, M. Mastellone, V. Serpente, V. Valentini, A. Bellucci, et al., Etching kinetics of nanodiamond seeds in the early stages of CVD diamond growth, ACS Omega 8 (2023) 25496–25505, https://doi.org/10.1021/acsomega.3c03080.
[49] J. Millán-Barba, M. Gutiérrez, F. Lloret, R.G. de Villoria, R. Alcántara, K. Haenen, et al., Study of early stages in the growth of boron-doped diamond on carbon fibers, Physica Status Solidi (A) Applications and Materials Science 218 (2021), https://doi.org/10.1002/pssa.202000284.
[50] B. Ma, S. Ren, P. Wang, C. Jia, X. Guo, Precise control of graphene etching by remote hydrogen plasma, Nano Res. 12 (2019) 137–142, https://doi.org/10.1007/s12274-018-2192-8.
[51] K. Yao, B. Dai, V. Ralchenko, G. Shu, J. Zhao, K. Liu, et al., Diamond films and particles growth in hydrogen microwave plasma with graphite solid precursor: optical emission spectroscopy study, Diam. Relat. Mater. 82 (2018) 33–40, https://doi.org/10.1016/j.diamond.2017.12.020.
[52] R. Yang, L. Zhang, Y. Wang, Z. Shi, D. Shi, H. Gao, et al., An anisotropic etching effect in the graphene basal plane, Adv. Mater. 22 (2010) 4014–4019, https://doi.org/10.1002/adma.201000618.
[53] D. Hug, S. Zihlmann, M.K. Rehmann, Y.B. Kalyoncu, T.N. Camenzind, L. Marot, et al., Anisotropic etching of graphite and graphene in a remote hydrogen plasma, npj 2D Mater. Appl. 1 (2017), https://doi.org/10.1038/s41699-017-0021-7.
[54] W. Li, D. Long, J. Miyawaki, W. Qiao, L. Ling, I. Mochida, et al., Structural features of polyacrylonitrile-based carbon fibers, J. Mater. Sci. 47 (2012) 919–928, https://doi.org/10.1007/s10853-011-5872-2.
[55] V. Mortet, Z.V. Živcová, A. Taylor, M. Davydová, O. Frank, P. Hubík, et al., Determination of atomic boron concentration in heavily boron-doped diamond by Raman spectroscopy, Diam. Relat. Mater. 93 (2019) 54–58, https://doi.org/10.1016/j.diamond.2019.01.028.
[56] V. Mortet, Z. Vlčková Živcová, A. Taylor, O. Frank, P. Hubík, D. Trémouilles, et al., Insight into boron-doped diamond Raman spectra characteristic features, Carbon N. Y. 115 (2017) 279–284, https://doi.org/10.1016/j.carbon.2017.01.022.
[57] D. Kumar, M. Chandran, M.S. Ramachandra Rao, Effect of boron doping on first-order Raman scattering in superconducting boron doped diamond films, Appl. Phys. Lett. 110 (2017), https://doi.org/10.1063/1.4982591.
[58] A.N. Utyuzh, YuA. Timofeev, A.V. Rakhmanina, Effect of boron impurity on the raman spectrum of synthetic diamond, Inorg. Mater. 40 (2004) 926–931, https://doi.org/10.1023.
[59] V. Mortet, A. Taylor, Z. Vlčková Živcová, D. Machon, O. Frank, P. Hubík, et al., Analysis of heavily boron-doped diamond Raman spectrum, Diam. Relat. Mater. 88 (2018) 163–166, https://doi.org/10.1016/j.diamond.2018.07.013.
[60] S. Prawer, R.J. Nemanich, Raman spectroscopy of diamond and doped diamond, Philos. Trans. R. Soc. A Math. Phys. Eng. Sci. 362 (2004) 2537–2565, https://doi.org/10.1098/rsta.2004.1451.
[61] M. Bernard, C. Baron, A. Deneuville, About the origin of the low wave number structures of the Raman spectra of heavily boron doped diamond films, Diam. Relat. Mater. 13 (2004) 896–899, https://doi.org/10.1016/j.diamond.2003.11.082.
[62] A.C. Ferrari, J. Robertson, Origin of the 1150 − cm<−1> Raman mode in nanocrystalline diamond, Phys. Rev. B Condens. Matter 63 (2001), https://doi.org/10.1103/PhysRevB.63.121405.
[63] V. Mortet, I. Gregora, A. Taylor, N. Lambert, P. Ashcheulov, Z. Gedeonova, et al., New perspectives for heavily boron-doped diamond Raman spectrum analysis, Carbon N. Y. 168 (2020) 319–327, https://doi.org/10.1016/j.carbon.2020.06.075.
[64] J. Hrabovsky, M. Zelensky, J. Sladek, M. Zukerstein, J. Fischer, K. Schwarzova-Peckova, et al., Laser-patterned boron-doped diamond electrodes with precise control of sp2/sp3 carbon lateral distribution, Appl. Surf. Sci. 639 (2023), https://doi.org/10.1016/j.apsusc.2023.158268.
[65] D.B. Williams, C.B. Carter, Transmission Electron Microscopy: a Textbook for Materials Science, second ed., Springer, New York, NY, 2009 https://doi.org/10.1007/978-0-387-76501-3.
[66] The Materials Project, 2020, https://doi.org/10.17188/1281384.